ingegneria sismica
International Journal of Earthquake Engineering
Anno XLII – Num.1 - 2025

RESEARCH ON SEISMIC STRUCTURAL OPTIMIZATION DESIGN BASED ON PERFORMANCE-BASED DESIGN METHODS

Noam W Buckley
University of Miami

SUMMARY: *Given the significant impact of seismic disasters, it is particularly important to apply performance-based design methods to building structures for seismic design. This paper first reviews the general methods for building structure design based on performance-based design, followed by a detailed design analysis of building structures using performance-based design methods. Finally, taking a specific building as an engineering example, performance-based design methods are applied to its structural design and analysis. Through the iterative changes in the stress ratio distribution of main components under multiple earthquake levels, it is found that the stress ratio of frame columns increases during the optimization process, with the proportion distributed between 0.6 and 1.0 increasing from 10% to 22%. This indicates that the performance-based design method proposed in this paper plays a positive role in enhancing the seismic performance of building structures.*

KEYWORDS: performance-based design, seismic structure, structural optimization, building

1 Introduction

Earthquakes are highly destructive natural disasters that cause significant loss of life and property to human society [1, 2]. To reduce earthquake damage to buildings and ensure public safety, seismic structural optimization design to enhance seismic performance is of utmost importance [3, 4].

Seismic structural optimization design requires a multi-faceted approach. First, appropriate structural selection is critical [5]. Common structural forms such as frame structures, shear wall structures, and frame-shear wall structures each have distinct seismic performance characteristics [6, 7]. Frame structures offer good flexibility but have relatively weaker seismic resistance [8]. Shear wall structures, on the other hand, possess strong lateral load-bearing capacity and are suitable for high-rise buildings [9]. Frame-shear wall structures combine the advantages of both, performing well under different loading conditions [10, 11]. When selecting a structural form, factors such as building height, use, and geographical location must be comprehensively considered [12, 13]. Foundation design is also a critical factor influencing seismic performance [14]. A well-designed foundation effectively distributes the load from the superstructure uniformly to the subgrade and maintains stability under seismic loads [15, 16] . Pile foundations, raft foundations, and other forms are common foundation types [17]. When designing foundations, it is essential to accurately assess the bearing capacity of the subgrade to

*noamwbuckley@gmail.com

ensure the foundation can withstand the horizontal and vertical forces generated by earthquakes [18, 19]. Material selection is equally critical for seismic performance [20]. High-strength, high-toughness building materials can enhance the structural bearing capacity and deformation capacity [21]. For example, adding an appropriate amount of fibers to concrete can enhance its tensile strength and improve its crack resistance [22]. The quality and performance of steel also directly affect the structural seismic resistance; selecting high-quality steel ensures the structure has sufficient ductility and energy dissipation capacity under seismic loads [23, 24].

Hassanzadeh, Moradi and Burton [25] points out that performance-based design optimization (PBDO) aims to design safe, resilient, and cost-effective structures, and reviews the rapidly developing field of PBDO and the evolution of PBDO methods, with the goal of identifying issues that need to be addressed in future research. Talatahari [26] introduces the optimal seismic design of steel frames based on four performance levels and uses meta-heuristic algorithms such as genetic algorithms and particle swarm optimization as advanced hybrid meta-heuristic methods. Gholizadeh [27] proposes a method incorporating two computational strategies for performance-based optimal seismic design of steel frames and introduces a new neural network model to validate the effectiveness of the aforementioned method. Gaxiola-Camacho et al. [28] proposes and successfully implements a unified performance-based seismic design program, which is validated through a series of studies and observations to demonstrate its robustness, efficiency, and accuracy. Degertekin, Tutar and Lamberti [29] discusses the application of a meta-heuristic method called "School Optimization" (SBO) in performance-based optimal seismic design of steel frames, revealing through testing that SBO design schemes are superior. Kaveh and Nasrollahi [30] discusses performance-based optimal seismic design of steel frames using the Charge System Search (CSS) optimization algorithm, demonstrating its superiority through comparison with traditional design methods. Guo [31] examines the characteristics, composition, and design requirements of high-rise intelligent buildings, and reviews their advantages and social benefits, emphasizing that further research and improvement are still needed to establish a performance-based reliability optimization decision-making model for high-rise intelligent buildings. Steneker et al. [32] implements a generic optimization program within the performance-based earthquake engineering (PBEE) framework using the Federal Emergency Management Agency's P-58 methodology. Through case studies, it demonstrates that genetic algorithms can determine different resource allocation schemes for structural and non-structural components.

The article first reviews structural design methods for high-rise buildings based on performance-based design approaches, systematically introducing general methods for high-rise building structural design. It proposes the use of a probability-based limit state design method grounded in reliability theory to ensure the structural reliability of buildings. Subsequently, it discusses the selection of the main structure, basement, and foundation for a specific building and evaluates the structural overlimit conditions. Subsequently, the method proposed in this paper is used to perform medium-seismic elastic verification of the structure. With the objective of minimizing steel usage in components, and constraints ensuring that indicators such as inter-story drift angle, component stress ratio, and damage grade do not exceed pre-set performance targets, the paper completes automatic iterative optimization of structural analysis, performance evaluation, and design adjustments.

2 Discussion on seismic structural design methods for buildings based on performance-based design methods

2.1 Building structural design

2.1.1 Probabilistic limit state design method

1. *Loads, Load Effects, and Structural Resistance.* A structure is a rational system composed of basic components with different functions connected in a reasonable and reliable manner, capable of safely and reliably withstanding various loads and fulfilling predetermined functional objectives during its anticipated service life [33]. Loads on a structure refer to concentrated and distributed forces applied to the structure, as well as various factors causing external deformation or constraint deformation of the structure. Structural resistance refers to the ability of the entire structure or structural components to withstand load effects.

2. *Reliability Theory.* The safety, serviceability, and durability of a structure are collectively referred to as structural reliability, which is the ability of a structure to fulfill its intended functions under specified conditions within a specified timeframe.

3. *Structural Functional Functions and Limit State Equations.* When designing building structures based on limit states, the design results must meet all predetermined functional requirements. The various functions of the structure are represented by functional functions $Z = g(X_1, X_2, X_3, \cdots X_n)$, when

$$Z = g(X_1, X_2, X_3, \cdots X_n) = 0. \tag{1}$$

   This is referred to as the limit state equation.

4. *Probabilistic limit state design method.*

   (a) The ultimate limit state refers to the condition where a structure or structural member reaches its maximum bearing capacity or undergoes deformation that renders it unsuitable for continued loading.

   For permanent design conditions, temporary design conditions, and seismic design conditions, when using the expression of internal forces, structural members should adopt the following limit state expressions:

$$\gamma_0 S \leq R, \tag{2}$$

   where, γ_0 os the structural importance coefficient, S is the design value of the effect of the action combination at the ultimate limit state of bearing capacity and R is the design value of structural member resistance.

   (b) Normal serviceability limit state refers to the state where the structure or structural member reaches a specified limit for normal use or durability performance.

   For normal serviceability limit states, load standard combinations, frequent combinations, or permanent combinations should be adopted according to different design requirements, and designed in accordance with the requirements of Eq. (3):

$$S \leq C, \tag{3}$$

where, S is the design value of the load combination effect of the normal serviceability limit state and C indicates the specified limit value for the structure or structural component to meet normal serviceability requirements.

2.1.2 Structural component design

For structures designed for seismic resistance, the load-bearing capacity of each component should meet the requirements of both Eq. (4) and Eq. (5). For permanent and temporary design conditions:

$$\gamma_0 S_d \leq R_d. \tag{4}$$

For seismic design conditions:

$$S_d \leq \frac{R_d}{\gamma_{RE}}, \tag{5}$$

where, R_d is the design value of component bearing capacity, S_d is the design value of load effect combination and γ_{RE} os seismic adjustment coefficient of component bearing capacity.

The cross-sections of shear wall members are typically rectangular, T-shaped, or I-shaped. At the ends of the cross-sections, structural edge members or restraining edge members are generally required to enhance their seismic performance.

The calculation of the normal section bearing capacity of wall members primarily involves the calculation of the normal section eccentric compression bearing capacity and the normal section eccentric tension bearing capacity [34].

For permanent and transient design conditions:

$$N \leq A_{s'} f_{y'} - A_s \sigma_s - N_{sw} + N_c, \tag{6}$$

$$N\left(e_0 + h_{w0} - \frac{h_w}{2}\right) \leq A_s^{'} f_y^{'}(h_{w0} - a_{s'}) - M_{sw} + M_c. \tag{7}$$

When subjected to eccentric tension, if the axial tensile force N is located between longitudinal reinforcing bars A_s and $A_s^{'}$, it is considered minor eccentric tension, and the entire cross-section is subjected to tension. Concrete cracks will penetrate the entire cross-section, so this minor eccentric tension situation should be avoided as much as possible.

For permanent and temporary design conditions:

$$N \leq \frac{1}{\frac{1}{N_{0u}} + \frac{e_0}{M_{wu}}}, \tag{8}$$

For seismic design conditions:

$$N \leq \frac{1}{\gamma_{RE}}\left(\frac{1}{\frac{1}{N_{0u}} + \frac{e_0}{M_{wu}}}\right), \tag{9}$$

$$N_{0u} = 2A_s f_y + A_{sw} f_{yw}, \tag{10}$$

$$M_{wu} = A_s f_y (h_{w0} - a_s^{'}) + A_{sw} f_{yw} \frac{(h_{w0} - a_s^{'})}{2}. \tag{11}$$

where, A_{sw} is thecross-sectional area of vertical distribution reinforcing bars in shear walls.

For seismic resistance grades I, II, and III, the shear design value of the reinforced bottom section of shear walls can be increased using an adjustment coefficient. For seismic resistance

grade IV and when there is no seismic action, no adjustment is necessary. The formula is as follows:

$$V = \eta_{vw} V_w, \tag{12}$$

where, V is the design value of shear force for the reinforced section at the bottom of the shear wall member under the combined seismic action, V_w is the calculated value of shear force for the reinforced section at the bottom of the shear wall member under the combined seismic action and η_{vw} is the shear force increase coefficient.

For permanent and temporary design conditions:

$$V \leq \frac{1}{\lambda - 0.5}\left(0.5 f_t b_w h_{w0} + 0.13 N \frac{A_w}{A}\right) + f_{yh}\frac{A_{sh}}{s} h_{w0}. \tag{13}$$

For seismic design conditions:

$$V \leq \frac{1}{\gamma_{RE}}\left[\frac{1}{\lambda - 0.5}\left(0.4 f_t b_w h_{w0} + 0.1 N \frac{A_w}{A}\right) + 0.8 f_{yh}\frac{A_{sh}}{s} h_{w0}\right], \tag{14}$$

where, N is the design value of axial pressure on the shear wall cross-section, A is the total cross-sectional area of the shear wall, A_w is the area of the web of a T-shaped or I-shaped shear wall cross-section; for rectangular cross-sections, take A, λ is the shear span ratio of the calculated cross-section and s is the spacing of horizontal distribution reinforcing bars in the shear wall.

In eccentrically loaded members, the adverse effects of axial tensile force are considered, and the axial force term is negative. The verification formula is similar to Eqs. (13) and (14), except that the tensile strength of concrete f_t replaces the compressive strength f_c, thereby changing the coefficient of the concrete term.

For permanent and temporary design conditions:

$$V \leq \frac{1}{\lambda - 0.5}\left(0.5 f_t b_w h_{w0} - 0.13 N \frac{A_w}{A}\right) + f_{yh}\frac{A_{sh}}{s} h_{w0}. \tag{15}$$

For seismic design conditions:

$$V \leq \frac{1}{\gamma_{RE}}\left[\frac{1}{\lambda - 0.5}\left(0.4 f_t b_w h_{w0} - 0.1 N \frac{A_w}{A}\right) + 0.8 f_{yh}\frac{A_{sh}}{s} h_{w0}\right]. \tag{16}$$

For column design, the design of the cross-section can be calculated based on the axial compression bearing capacity or the eccentric compression bearing capacity. Eccentric compression columns exhibit two primary failure characteristics depending on the eccentricity of the axial force N relative to the cross-section e_0 and the longitudinal reinforcement ratio: tensile failure and compressive failure.

When calculating the normal section bearing capacity of beams, depending on the cross-sectional shape of the beam, the normal section bearing capacity of single-reinforced rectangular cross-section beams and double-reinforced rectangular cross-section beams is calculated separately.

The slab still experiences a certain amount of bending moment and bending deformation at the intersection with the main beam, so a certain amount of structural reinforcement should be provided at this location. The design of one-way slab rib-beam floor systems mainly involves positive section bearing capacity calculation and oblique section bearing capacity calculation.

Shear bearing capacity calculations must be performed for the core areas of first-, second-, and third-level frame nodes. Sufficient horizontal stirrups must be configured within the nodes to ensure that shear failure does not occur.

2.2 Structural overview

2.2.1 Structural geometric information

The structure has a height of 255.3 m, a plan dimension of $47.8\text{m}^3 \times 39.0\text{m}$, a length-to-width ratio of 1.29, a height-to-width ratio of 7.80, a core tube dimension of $25.2\text{m}^3 \times 16.7\text{m}$, and a core tube height-to-width ratio of 16.3.

2.2.2 Structural selection

Considering factors such as building floor plan functionality, facade design, seismic (wind) performance requirements, construction schedule, and cost-effectiveness, the structural system adopts a reinforced concrete frame-core wall structure. In the reinforced zone at the bottom of the building, high-ductility components are used for critical structural elements, while the outer frame employs steel-reinforced concrete columns to enhance vertical component load-bearing capacity and seismic ductility [35]. The lateral resistance system consists of the outer frame and core tube, forming a multi-layered seismic-resistant structural system that provides the necessary gravity load-bearing capacity and lateral stiffness. Gravity loads are transmitted through floor horizontal components to the core tube and outer frame columns, and ultimately to the foundation. Shear forces and overturning moments generated by horizontal loads are shared by the outer frame and core tube. Shear forces are primarily borne by the core tube, while overturning moments are shared by both the core tube and outer frame. The structural design achieves the building's "bamboo" façade by varying the cantilever length of the perimeter beams, while the main structural frame columns and core tube remain continuously upright.

2.2.3 Structural arrangement

1. *Floor Slab System.* The floor structure of the office building adopts a cast-in-place reinforced concrete main and secondary beam system. In the sections of the outer frame columns and core tube where vertical compression deformation is greatest, horizontal bracing segments are installed at the beam supports connecting the outer frame columns to the core tube. The advantage of horizontal bracing lies in its ability to enhance component ductility without significantly increasing component stiffness, effectively alleviating the issue of excessively high stress levels at the ends of frame beams in concrete structures used in super-high-rise buildings. This is caused by horizontal loads and vertical deformation differences between the outer frame and inner core, which can make it difficult to meet seismic ductility requirements. Additionally, horizontal bracing is one of the measures to reduce structural self-weight and mitigate seismic load effects.

2. *Main Component Dimensions.* The cross-sections and bracing conditions of frame beams between frame columns and core cylinders are shown in Table 1 (frame beams in the X-direction have no bracing, corner frame beams have no column-end bracing, and blank spaces in the table indicate no bracing).

2.2.4 Basement and foundation

1. *Basement Structural System.* The basement of a certain office building is part of the overall basement of the central plot and constitutes an integral structural unit. The basement

Table 1: Frame beam dimensions

Floor range	X to frame beam main section	Y-direction frame beam			Corner frame beam	
		Principal section	Add axils at the end of the column	Add axils to the end of the cylinder	Principal section	Simply add the armpit to the tip
Floors 2 to 5	450×900	450×900			450×900	
Floors 6 to 14	600×700	600×700			600×700	
15th floor (Refuge floor)	900×700	900×700			900×700	1000×700
Floors 16 to 30	450×700	600×700	900×700	900×700	450×700	900×700
31th floor (Refuge floor)	900×700	900×700			900×700	1200×700
32nd floor	600×700	600×700	900×700	900×700	600×700	900×700
Floors 33 to 44	600×700	600×700		900×700	600×700	900×700
Floors 45 to 46	450×700	450×700			600×700	
47th floor	900×700	900×700			900×700	
48th floor	450×700	450×700			450×700	900×700
49∼ Roof layer	450×700	450×700			450×700	

has three levels, primarily designed as a wartime civil defense shelter. The structural layout of the civil defense-designated floors is detailed in separate civil defense-specific drawings. In peacetime, the basement is used as a garage and equipment rooms. The area within the tower's projection is an extension of the tower's structural system and follows a frame-core wall structural system. The area outside the tower's projection consists of standard basement side walls, frame beams, columns, and floor slabs, forming a standard frame structural system. Basement floor system selection:

2. *Basement Foundation Selection.*

   (a) *Floatation Water Level.*

      i. ±0.00m (relative elevation) = 4.30m (absolute elevation).

      ii. Absolute elevation of the basement floor slab = -8.00m.

      iii. The elevation for the buoyancy-resistant waterproofing level is determined based on the outdoor pavement elevation. When the building's burial depth is approximately 14m, if the gradient of the outdoor pavement elevation change is less than 2m, the average value is taken; if the outdoor pavement elevation change exceeds 3m, segmented values are taken.

   (b) Geological conditions and foundation selection are determined based on the geological conditions revealed by drilling:

      i. The elevation of strongly weathered rock surfaces is relatively shallow, with a significant portion of the site area having a depth from the strongly weathered rock surface to the foundation slab bottom of less than 8 meters. Therefore, prestressed pipe piles are not suitable for pure basement column foundations controlled by uplift resistance.

      ii. The thickness of the strongly weathered layer is relatively thin, with a significant portion of the site area having a thickness between 2 and 4 meters. The base of the strongly weathered layer is the moderately weathered layer of hard granite. The columns of the tower and the core tube are proposed to use large-diameter manually excavated cast-in-place piles.

      iii. In response to the above points 1 and 2, the column foundations for the purely underground portion are controlled by uplift resistance. To meet the uplift resistance bearing capacity requirements, the same large-diameter manually excavated cast-in-place pile foundation form is adopted.

   (c) *Bottom Slab Buoyancy Resistance.* The basement is buried at a depth of approximately 14 m, with a buoyancy resistance water level as high as 11.2 m. Based on its self-waterproofing and basic waterproofing requirements, combined with the

basement column span conditions, the value is set at 900 mm. The bottom slab structure uses a 900 mm thick beamless bottom slab. For areas with high stress under columns, solutions such as adding axillary supports to the base of the cap or expanding the cap are adopted.

2.2.5 Seismic resistance rating

The seismic design category is Class B. Seismic measures are based on a seismic intensity of 8 degrees, one degree higher than the design intensity. The height of 260 meters falls under the super-B-class height for frame-core wall structures. The seismic resistance grade is determined in accordance with Article 3.9.4 of the Guangdong Province "Technical Specifications for Concrete Structures of High-Rise Buildings." The frame is classified as Grade 1, and the core tube is classified as Special Grade 1. Considering the super-B-class height factor, the seismic resistance grade of the frame is increased by one level for the bottom reinforcement zone of shear walls below the 7th floor, and Special Grade 1 is adopted as one of the structural reinforcement measures. The structural seismic resistance grades are shown in Table 2. Considering that the projected area of the tower occupies more than 80% of the basement floor plan, the seismic resistance grade classification no longer distinguishes between areas within and outside the relevant range, but uniformly adopts the seismic resistance grade within the relevant range as one of the structural reinforcement measures.

Table 2: Structural seismic resistance grade

Component position		Framework	Core tube
Main tower	7 floors and above	First class	first-class
	The first layer of ~ 6	first-class	first-class
	Underground layer	first-class	first-class
	sublayer	First class	First class
	Underground layer	Second class	Second class
The basement of the main tower tower	The first to third floors underground	The corresponding floor frame grade of the same tower area	

3 Structural design of a specific engineering project based on performance-based design methods

3.1 Seismic performance design under seismic action

3.1.1 Medium-intensity seismic elasticity verification

1. *Shear Wall Axial Compression Ratio.* The axial compression ratio is a key factor influencing the plastic deformation capacity of shear walls under seismic loads. Under identical conditions, shear walls with lower axial compression ratios exhibit greater ductility, while those with higher ratios exhibit lesser ductility. According to Clause 4.2.13 of the High-Rise Building Code, the axial compression ratio limit for shear wall members under the representative value of gravity loads is 0.5. Typical wall member numbers are shown in Figure 1, which illustrates the axial compression ratios of the lower-level structure. The maximum axial compression ratio of the bottom wall members is approximately 0.40, which still has a certain margin relative to the code limit, ensuring good ductility of the wall members from the perspective of axial compression ratio.

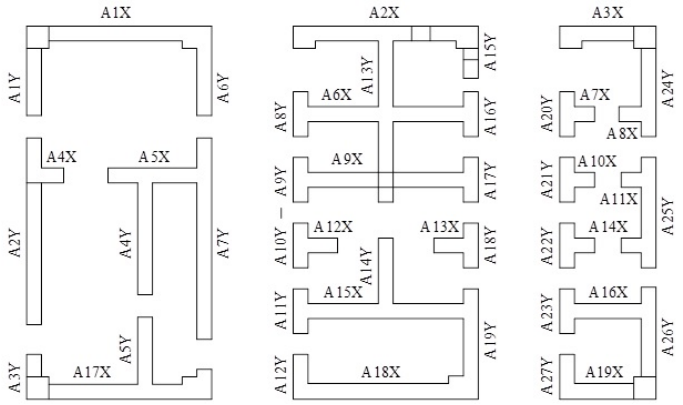

Figure 1: Wall limb numbering

2. *Tensile Design of Frame Columns and Shear Walls.* The axial force at the bottom of the wall under seismic conditions in some shorter wall sections is shown in Table 3. No tensile stress was observed in the bottom wall of the core cylinder.

Table 3: Axial force and tensile stress of the bottom wall under moderate seismic conditions

Wall number	The gravity load represents the shaft force at (1.0d+ 0.5l) (kN)	The N_{max}(kN) of the unyielding condition of the middle	The N_{min}(kN) of the unyielding condition of the middle	The stress of the vibration wall (Mpa)
A1y(3300×500)	-19549	-15165	9722	No
A3y(1000×500)	-7547	-12219	3993	No
A6y(2950×400)	-15025	-17417	3982	No
A10y(1450×400)	-7288	-8480	1059	No
A13y(7225×300)	-22268	-25852	-639	No
A18y(1450×400)	-7274	-8452	1523	No
A20y(1450×400)	-7142	-8253	-594	No
A21y(1450×400)	-7094	-8214	-206	No
A7x(825×200)	-2358	-2753	-287	No
A8x(825×200)	-2398	-2775	-246	No
A10x(825×200)	-2315	-2685	-62	No
A11x(825×200)	-2472	-2854	-63	No
A12x(825×200)	-1992	-2313	203	No
A13x(825×200)	-1969	-2279	306	No

3. *Shear Verification of Shear Walls in the Reinforced Zone at the Bottom (moderate seismic elasticity).* The shear bearing capacity and shear performance of the shear walls in the reinforced zone at the bottom of this project are designed according to moderate seismic elasticity, in accordance with the "key component shear elasticity" required by the predetermined seismic performance target. The internal forces of typical wall members in the main building's SATWE model were extracted using the moderate earthquake response spectrum method. The shear capacity of the shear walls under eccentric compression and tension conditions was verified. The shear-to-compression ratio verification results for all wall members were less than 0.15, and the shear capacity/shear force/0.85 ratio was greater than 1. The shear capacity of the shear walls meets the moderate earthquake elasticity requirements. The shear capacity verification of the shear walls (moderate earthquake elasticity) is shown in Table 4.

3.1.2 Trends in the seismic load-bearing capacity of the overall structure

The capacity spectra and performance point curves under various seismic conditions are shown in Figure 2 (Figures a and b represent the performance curves and performance points in the X and Y directions, respectively). As can be seen from the figure, under small seismic conditions, the structure is in the elastic stage, and the spectral displacement and spectral acceleration are linearly related. Under medium seismic conditions, the structure is still in the elastic state, but the overall seismic bearing capacity is on an upward curve and has not decreased.

Table 4: Shear wall shear resistance verification (moderate seismic elasticity)

Wall number	Bending moment(kN·M)	Axial force(kN)	Shear force(kN)	fcbwhw0	Shear ratio	Shear capacity	Shear bearing capacity/Shear force/0.85
A1y(3300×500)	3758	-22678	2446	45026	0.05	3698	1.8
A3y(1000×500)	1601	-12211	431	13409	0.03	935	2.6
A6y(2950×400)	2196	-17431	1950	32162	0.06	2973	1.8
A10y(1450×400)	724	-8485	510	15680	0.03	1368	3.2
A18y(1450×400)	694	-8440	532	15680	0.03	1377	3.0
A20y(1450×400)	757	-8266	489	15680	0.03	1327	3.2
A21y(1450×400)	501	-8196	323	15680	0.02	1329	4.8
A7x(825×200)	290	-2752	114	4500	0.02	298	3.1
A8x(825×200)	113	-2764	77	4500	0.02	429	6.6
A10x(825×200)	206	-2677	63	4500	0.02	310	5.8
A11x(825×200)	145	-2837	78	4500	0.02	365	5.5
A12x(825×200)	25	-2317	36	4500	0.01	441	14.4
A13x(825×200)	21	-2255	29	4500	0.01	440	17.8

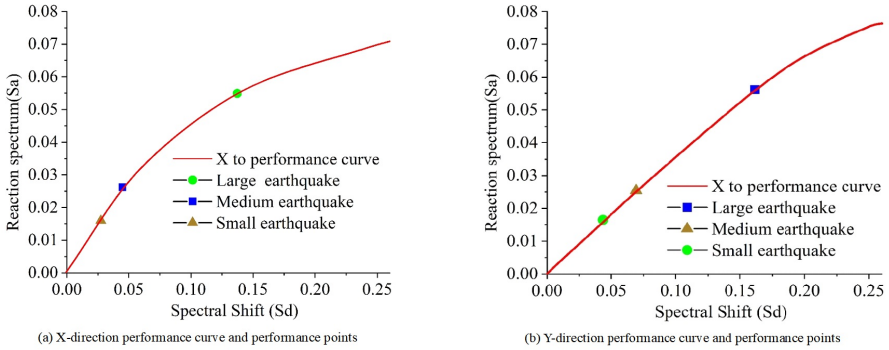

Figure 2: Performance point results at different seismic levels in the X and Y directions

The performance point results for X and Y directions under different seismic levels are shown in Table 5. The medium seismic performance points indicate that the structure remains elastic, while the effective damping is relatively large during a major earthquake, indicating that the structure has good energy dissipation capabilities.

Table 5: Performance point results at different seismic levels in the X and Y directions

Direction	Level	Maximum displacement Angle	Steps/General steps	Base shear force	Maximum displacement	Effective damping ratio
X direction	Small earthquake	1/2069	2/32	1.11E+04	0.06549	4
	Medium shock	1/1282	4/32	1.66E+04	0.09885	4
	Large seismic magnitude	1/453	14/32	3.45E+04	0.1912	8.642
Y direction	Small earthquake	1/2041	2/46	1.14E+04	0.05	4
	Medium shock	1/1203	3/46	1.72E+04	0.1044	4
	Large seismic magnitude	1/400	15/46	3.94E+04	0.238	7.251

3.2 Design results

The iterative curves and distribution of inter-story displacement angles under rare earthquakes are shown in Figure 3. During the iterative optimization process, the maximum inter-story displacement angle of the structure decreased from 1/84 to 1/90, while the inter-story displacement angle of the first floor increased from 1/162 to 1/119, both of which met the preset performance target requirements.

The iteration of base shear under rare earthquake levels is shown in Figure 4. During the iteration process, the structural mass decreases and the support cross-section decreases, causing the base shear reflecting the input seismic action to decrease continuously.

The iterative changes in the stress ratio distribution of major components under multiple earthquake levels are shown in Figure 5 (Figures a–c represent frame columns, frame beams,

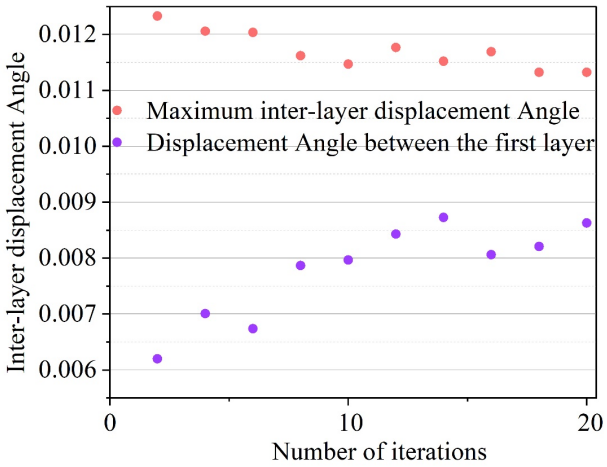

Figure 3: Iteration of inter-storey drifts

and supports, respectively). It can be seen that after optimization, the stress ratios of frame columns and frame beams are mainly distributed between 0.2 and 0.8 and between 0 and 0.6, respectively. The stress ratios of braces are mostly greater than 0.6. During the optimization process, the stress ratio of frame columns increased slightly, with the proportion distributed between 0.6 and 1.0 rising from 10% to 22%. The stress ratio of braces increased significantly, with the proportion distributed between 0.8 and 1.0 rising from 10% to 78%. The stress ratio distribution of frame beams changed little.

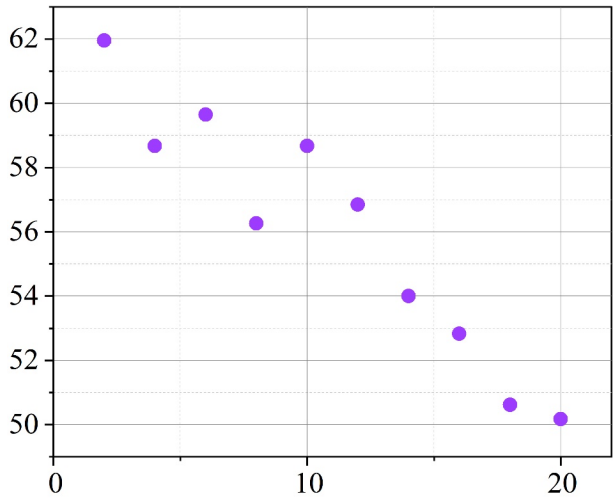

Figure 4: Shear force iteration of the structural base

The iterative changes in the distribution of damage severity of major structural components under rare earthquake conditions are shown in Figure 6. It can be seen that after optimization, the overall damage severity of the structure is relatively low, with 99% of the frame columns and frame beams not exceeding minor damage, and the supports not exceeding moderate damage. During the optimization process, the proportion of frame columns exceeding moderate damage decreased from 0.6% to 0%. The proportion of supports in a mild damage state gradually increased from 70% to 85%. The distribution of damage severity for frame beams remained largely unchanged.

The statistical results of the component performance evaluation are shown in Table 6. It can

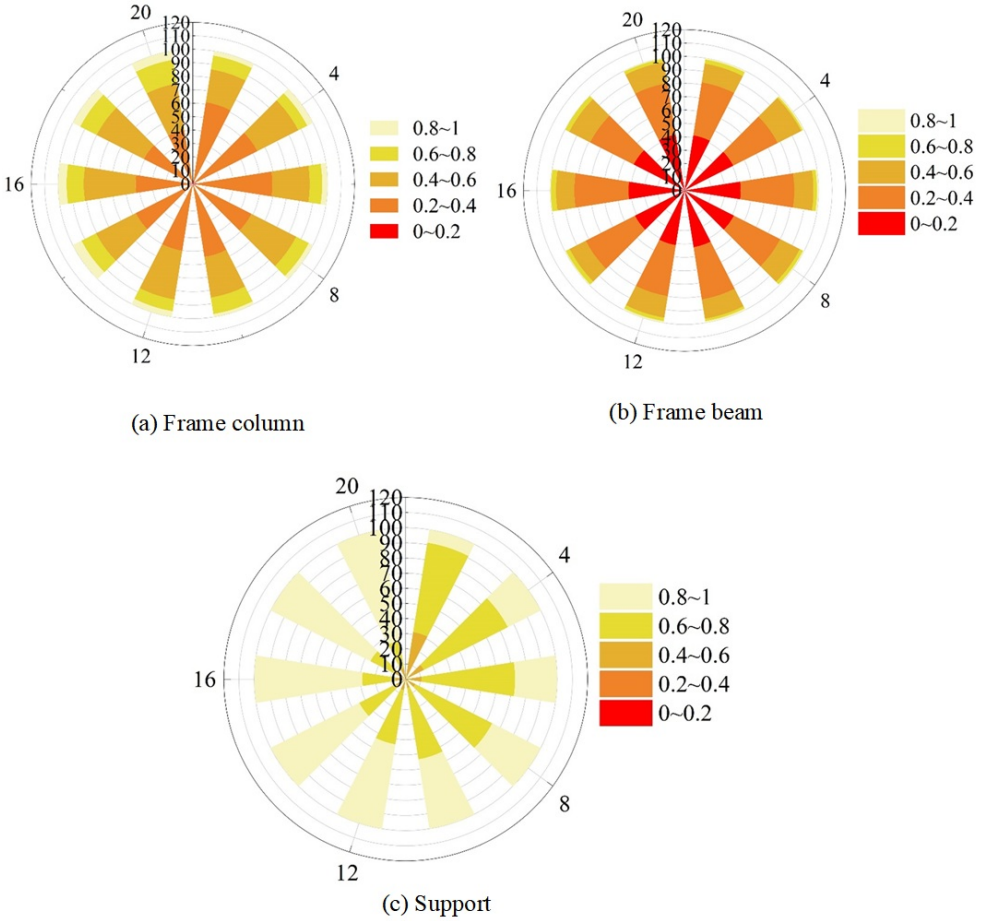

Figure 5: Iteration of stress ratio distribution

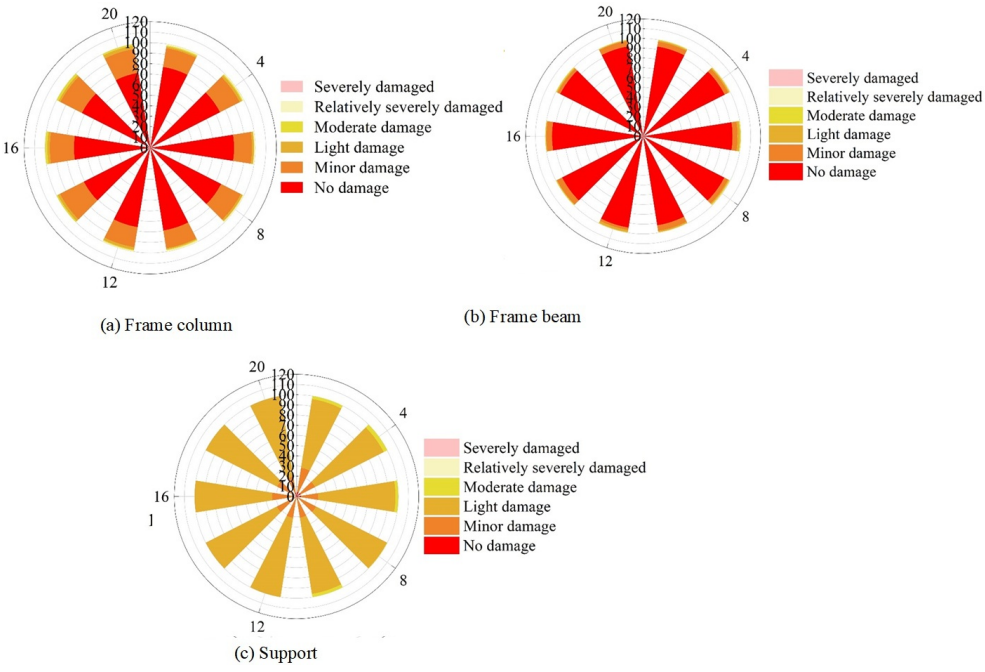

Figure 6: Iteration of component damage grade distribution

be seen that after optimization, all structural components meet the preset performance target requirements.

Table 6: Results of component performance evaluation

Member type		Frequent earthquakes			Rare earthquakes		
		Maximum stress ratio	Limit value	Satisfied	Degree of damage	Limit value	Satisfied
Frame column	Support span	0.86	Non-destructive damage($\leq$0.81)	√	Moderate damage	Not exceeding moderate damage	√
	Non-support span	0.75	Non-destructive damage($\leq$0.93)	√	Minor damage	Not exceeding moderate damage	√
Frame beam	Support span	0.66	Non-destructive damage($\leq$0.81)	√	Minor damage	Not exceeding moderate damage	√
	Non-support span	0.74	Non-destructive damage($\leq$0.93)	√	Moderate damage	It does not exceed relatively serious damage	√
Central support		0.96	Non-destructive damage($\leq$0.95)	Non-destructive damage	Minor damage	It does not exceed relatively serious damage	√

3.3 Certain building structure design

Through computational analysis of the structure under seismic loads, the internal forces and deformations of the structure are determined. During structural design, reinforcement is specified based on the envelope of the results from frequent earthquakes and design earthquakes. Additionally, considering the primary measures for handling structural members exceeding limits under rare earthquakes, the reinforcement design of structural components is carried out.

The wall sections are made of C50 concrete, with $f_c = 23.1\,\mathrm{N/mm^2}$, $f_t = 1.89\,\mathrm{N/mm^2}$. The section dimensions are:

$$h_w = 2500\,\mathrm{mm}, \quad b_w = 500\,\mathrm{mm}, \quad b'_f = 1000\,\mathrm{mm}, \quad h'_f = 1000\,\mathrm{mm},$$

$$a_s = a'_s = 500\,\mathrm{mm}, \quad h_{w0} = h_w - a'_s = 1800\,\mathrm{mm}.$$

The distribution reinforcement and main reinforcement use HRB400 steel, $f_{yw} = 380\,\mathrm{N/mm^2}$.

The most unfavorable internal forces in seismic design are:

$$M = 1672.7\,\mathrm{kN\cdot m}, \quad N = 10631.5\,\mathrm{kN}, \quad V = 1295.6\,\mathrm{kN}.$$

The axial compression ratio is given by

$$\mu_v = \frac{N}{b_w h_w f_c} = \frac{10631.5 \times 10^3}{500 \times 2500 \times 23.1} = 0.51 < 0.6,$$

which meets the requirements.

The shear span ratio is

$$\lambda = \frac{M}{V h_{w0}} = \frac{1672.7 \times 10^6}{(1295.6/1.4) \times 10^3 \times 1800} = 0.91 < 2.5.$$

The capacity condition is satisfied since

$$\frac{1}{\gamma_{RE}}(0.15\beta_c f_c b_w h_{w0}) = 3092.12\,\mathrm{kN} > 1290.1\,\mathrm{kN}.$$

The vertical reinforcing bars for the wall are configured as C10@100.

$$\rho_{sw} = \frac{2 \times 0.785}{40 \times 10} = 0.393\% > 0.25\%,$$

which meets the requirements.

A preliminary estimate of the neutral axis depth gives

$$x = \frac{\gamma_{RE} N}{\alpha_1 f_c b'_f} = \frac{0.85 \times 10631.5 \times 10^3}{1.0 \times 23.1 \times 1000} = 391.2\,\text{mm} < h'_f = 1000\,\text{mm}.$$

Refined calculation:

$$x = \frac{\gamma_{RE} N + h_{w0} b_w \rho_w f_{yw}}{\alpha_1 f_c b'_f + 1.5 b_w \rho_w f_{yw}} = 412.57\,\text{mm},$$

$$\xi = \frac{x}{h_{w0}} = 0.2166 < \xi_b = 0.522.$$

Thus, the section is in large eccentric compression. The contributions are

$$M_{sw} = \tfrac{1}{2}(h_{w0} - 1.5x)^2 b_w \rho_w f_{yw} = 295.12\,\text{kN}\cdot\text{m},$$

$$M_c = \alpha_1 f_c b'_f x \left(h_{w0} - \tfrac{x}{2}\right) = 1611.1\,\text{kN}\cdot\text{m}.$$

The eccentricity is

$$e_0 = \frac{M}{N} = \frac{1689.7}{10644.5} = 158.7\,\text{mm},$$

$$e_0 + h_{w0} - \tfrac{h_w}{2} = 857.1\,\text{mm}.$$

The reinforcement area required is

$$A_s = \frac{\gamma_{RE} N \left(e_0 + h_{w0} - \frac{h_w}{2}\right) + M_{sw} - M_c}{f'_y (h_{w0} - a'_s)} = 12875\,\text{mm}^2.$$

The minimum longitudinal reinforcement area is $A_{s,\min} = 10800\,\text{mm}^2$. Adopting 30C25 bars gives $14727\,\text{mm}^2$, which satisfies requirements. End column stirrups are C10@100.

For shear wall horizontal reinforcement,

$$0.2 f_c b_w h_w = 0.2 \times 23.2 \times 400 \times 2400 = 4452.1\,\text{kN} < N,$$

so $N = 4435.2\,\text{kN}$ is used. Horizontal distribution reinforcement: C10@100.

For the no-seismic load case:

$$M = 1235.9\,\text{kN}\cdot\text{m}, \quad V = 140.9\,\text{kN}.$$

At $0.5h_{w0}$ from the base:

$$M = 415.1\,\text{kN}\cdot\text{m}, \quad V = 369.2\,\text{kN},$$

$$\lambda = \frac{M}{V h_{w0}} = \frac{415.1 \times 10^6}{369.2 \times 10^3 \times 1900} = 0.626 < 1.5.$$

The shear resistance is

$$\begin{aligned}[V_w] &= \frac{1}{\lambda - 0.5}\left(0.5 f_t b_w h_{w0} + 0.13 N \frac{A_w}{A}\right) + f_{yh}\frac{A_{sh}}{s} h_{w0} \\ &= \left(0.5 \times 1.89 \times 400 \times 1900 + 0.13 \times 4435.2 \times 10^3 \tfrac{0.56}{1.56}\right) \\ &\quad + 360 \times \tfrac{157}{100} \times 1900 \\ &= 1998.05\,\text{kN} > 140.9\,\text{kN}.\end{aligned}$$

For the seismic load case:

$$M = 651.5\,\text{kN}\cdot\text{m}, \quad V = 141.6\,\text{kN},$$

$$\lambda = \frac{M}{Vh_{w0}} = \frac{651.5\times10^6}{141.6\times10^3\times1900} = 2.41 > 2.2.$$

Hence, with $\lambda = 2.2$:

$$\begin{aligned}[V_w] &= \frac{1}{\gamma_{RE}}\left[\frac{1}{\lambda-0.5}\left(0.4f_t b_w h_{w0} + 0.1N\frac{A_w}{A}\right) + 0.8f_{yh}\frac{A_{sh}}{s}h_{w0}\right] \\ &= \tfrac{1}{0.85}\left[\tfrac{1}{2.2-0.5}\left(0.4\times1.89\times400\times1900 + 0.1\times4435.2\times10^3\tfrac{0.56}{1.56}\right)\right. \\ &\qquad \left.+0.8\times360\times\tfrac{157}{100}\times1900\right] \\ &= 1358.9\,\text{kN} > 1290.1\,\text{kN}.\end{aligned}$$

Thus, the shear design also meets the requirements.

4 Conclusion

In recent years, with the development of socio-economic and engineering technologies, performance-based seismic design methods have provided reliable and comprehensive solutions for building structural design through more targeted defense objectives and refined analysis and calculations. This paper proposes a performance-based design method and uses a specific building project as an example to illustrate the effectiveness of this method. The conclusions reached are as follows:

1. In the capacity spectrum and performance point analysis under various seismic conditions, under moderate seismic conditions, the building structure remains in an elastic state, and the overall seismic bearing capacity is on an upward curve.

2. In iterative experiments on the distribution of damage severity in primary components under rare earthquake levels, during the optimization process, the proportion of frame columns exceeding moderate damage decreased from 0.6% to 0%. The distribution of damage severity in the overall frame beams remained largely unchanged.

Hence, the building structures designed using the method described in this paper exhibit excellent seismic resistance.

References

[1] Bayram, H., Rastgeldi Dogan, T., Şahin, Ü. A., & Akdis, C. A. (2023). Environmental and health hazards by massive earthquakes. *Allergy, 78*(8), 2081-2084.

[2] Fan, X., Scaringi, G., Korup, O., West, A. J., van Westen, C. J., Tanyas, H., ... & Huang, R. (2019). Earthquake-induced chains of geologic hazards: Patterns, mechanisms, and impacts. *Reviews of Geophysics, 57*(2), 421-503.

[3] Li, S., Yu, B., Gao, M., & Zhai, C. (2019). Optimum seismic design of multi-story buildings for increasing collapse resistant capacity. *Soil Dynamics and Earthquake Engineering, 116*, 495-510.

[4] Montuori, R., Nastri, E., & Piluso, V. (2022). Theory of plastic mechanism control: A new approach for the optimization of seismic resistant steel frames. *Earthquake Engineering & Structural Dynamics, 51*(15), 3598-3619.

[5] Wang, J., & Zhao, H. (2018). High performance damage-resistant seismic resistant structural systems for sustainable and resilient city: A review. *Shock and Vibration, 2018*(1), 8703697.

[6] Foraboschi, P. (2020). Optimal design of seismic resistant RC columns. *Materials, 13*(8), 1919.

[7] Aktaş, Y. D. (2017). Seismic resistance of traditional timber-frame hımış structures in Turkey: a brief overview. *International Wood Products Journal, 8*(1_suppl), 21-28.

[8] Dubina, D., Stratan, A., Vulcu, C., & Ciutina, A. (2014). High strength steel in seismic resistant building frames. *Steel Construction, 7*(3), 173-177.

[9] Vetr, M. G., Shirali, N. M., & Ghamari, A. (2016). Seismic resistance of hybrid shear wall (HSW) systems. *Journal of Constructional Steel Research, 116*, 247-270.

[10] Vijayan, V., Santhi, M. H., & Mohan, R. (2020, September). Seismic performance of high rise buildings with different types of shear wall. In *IOP Conference Series: Materials Science and Engineering* (Vol. 936, No. 1, p. 012055). IOP Publishing.

[11] Sun, X., He, M., Li, Z., & Lam, F. (2019). Seismic performance assessment of conventional CLT shear wall structures and post-tensioned CLT shear wall structures. *Engineering Structures, 196*, 109285.

[12] Kurama, Y. C., Sritharan, S., Fleischman, R. B., Restrepo, J. I., Henry, R. S., Cleland, N. M., ... & Bonelli, P. (2018). Seismic-resistant precast concrete structures: State of the art. *Journal of Structural Engineering, 144*(4), 03118001.

[13] Bai, J., Jin, S., & Ou, J. (2020). An efficient method for optimizing the seismic resistance of reinforced concrete frame structures. *Advances in Structural Engineering, 23*(4), 670-686.

[14] Barmenkova, E. (2019, November). Design of Base and Foundation for the Earthquake-Resistant Building. In *IOP Conference Series: Materials Science and Engineering* (Vol. 661, No. 1, p. 012093). IOP Publishing.

[15] Shahjalal, M., Yahia, A. K. M., Morshed, A. S. M., & Tanha, N. I. (2024). Earthquake-resistant building design: Innovations and challenges. *Global Mainstream Journal of Innovation, Engineering & Emerging Technology, 3*(04), 101-119.

[16] Belash, T. A., & Ivanova, T. V. (2020). Earthquake resistance of buildings on thawing permafrost grounds. *Magazine of Civil Engineering*, (1 (93)), 50-59.

[17] Rambabu, R., Ramanjaneyulu, B., & Mahesh, K. (2024). Base isolation and energy dissipating system in earthquake resistant building design. *CVR Journal of Science and Technology, 26*(1), 13-20.

[18] Turdikulov, K. (2024). Calculation and design of earthquake resistant grounds. *Western European Journal of Modern Experiments and Scientific Methods, 2*(6), 144-150.

[19] Dražić, J., & Vatin, N. (2016). The influence of configuration on to the seismic resistance of a building. *Procedia Engineering, 165,* 883-890.

[20] Vandanapu, S. N., & Krishnamurthy, M. (2018). Seismic performance of lightweight concrete structures. *Advances in Civil Engineering, 2018*(1), 2105784.

[21] Bertero, V. V. (2019). Performance-based seismic engineering: A critical review of proposed guidelines. *Seismic Design Methodologies for the Next Generation of Codes*, 1-31

[22] Tian, P., Yang, W., Cao, C., Bian, Z., Yun, Z., & Lu, J. (2024, October). A study of the seismic resistance performance of strengthened masonry walls using polypropylene mesh-composite on the surface. In *Structures* (Vol. 68, p. 107270). Elsevier.

[23] Morrison, M., Schweizer, D., & Hassan, T. (2015). An innovative seismic performance enhancement technique for steel building moment resisting connections. *Journal of Constructional Steel Research, 109*, 34-46.

[24] Wang, M., Zhang, C., Sun, Y., & Dong, K. (2022). Seismic performance of steel frame with replaceable low yield point steel connection components and the effect of structural fuses. *Journal of Building Engineering, 47*, 103862.

[25] Hassanzadeh, A., Moradi, S., & Burton, H. V. (2024). Performance-based design optimization of structures: state-of-the-art review. *Journal of Structural Engineering, 150*(8), 03124001.

[26] Talatahari, S. (2013). Optimum performance-based seismic design of frames using metaheuristic optimization algorithms. *Metaheuristic Applications in Structures and Infrastructures, 45*(2), 419-437.

[27] Gholizadeh, S. (2015). Performance-based optimum seismic design of steel structures by a modified firefly algorithm and a new neural network. *Advances in Engineering Software, 81*, 50-65.

[28] Gaxiola-Camacho, J. R., Azizsoltani, H., Villegas-Mercado, F. J., & Haldar, A. (2017). A novel reliability technique for implementation of performance-based seismic design of structures. *Engineering Structures, 142*, 137-147.

[29] Degertekin, S. O., Tutar, H., & Lamberti, L. (2021). School-based optimization for performance-based optimum seismic design of steel frames. *Engineering with Computers, 37*(4), 3283-3297.

[30] Kaveh, A., & Nasrollahi, A. (2014). Performance-based seismic design of steel frames utilizing charged system search optimization. *Applied Soft Computing, 22*, 213-221.

[31] Guo, C. (2020, July). Performance-based structural seismic method in high-rise building design. In *Journal of Physics: Conference Series* (Vol. 1578, No. 1, p. 012190). IOP Publishing.

[32] Steneker, P., Filiatrault, A., Wiebe, L., & Konstantinidis, D. (2020). Integrated structural–nonstructural performance-based seismic design and retrofit optimization of buildings. *Journal of Structural Engineering, 146*(8), 04020141.

[33] Park, D., Kim, H. M., Ryu, D. W., Song, W. K., & Sunwoo, C. (2012). Application of a point estimate method to the probabilistic limit-state design of underground structures. *International Journal of Rock Mechanics and Mining Sciences, 51*, 97-104.

[34] Jiang, C., Yan, Y., Wang, D., Qiu, H., & Gao, L. (2021). Global and local Kriging limit state approximation for time-dependent reliability-based design optimization through wrong-classification probability. *Reliability Engineering & System Safety, 208*, 107431.

[35] Bours, A. L., & Knobloch, M. (2025). Stability Design of Two-Span Steel Members: Experimental Study on the Structural Performance and Detailing of the Central Support. *Journal of Structural Engineering, 151*(9), 04025130.